Solar Physics (2005) 231: 71–85

RELATING WHITE-LIGHT CORONAL IMAGES TO MAGNETIC FIELDS AND PLASMA FLOW

RICHARD WOO
Jet Propulsion Laboratory, California Institute of Technology, 4800 Oak Grove Drive, MS 238-725, Pasadena, CA 91109, U.S.A.

(Received 12 January 2004; accepted 6 May 2005)

Abstract. The solar magnetic field is key to a detailed understanding of the Sun's atmosphere and its transition to the solar wind. However, the lack of detailed magnetic field measurements everywhere except at the photosphere has made it challenging to determine its topology and to understand how it produces the observed plasma properties of the corona and solar wind. Recent progress based on the synthesis of diversified observations has shown that the corona is highly filamentary, that the coronal magnetic field is predominantly radial, and that the ability of closed fields to trap plasma at the base of the corona is a manifestation of how the solar field controls the solar wind. In this paper, we explain how these results are consistent with the relationship between density structure of white-light images and fields and flow. We point out that the 'shape' of the corona observed in white-light images is a consequence of the steep fall-off in density with radial distance, coupled with the inherent limitation in the sensitivity of the observing instrument. We discuss how the significant variation in radial density fall-off with latitude leads to a coronal shape that is more precisely revealed when a radial gradient filter is used, but which also gives a false impression of the tracing of highly non-radial fields. Instead, the coronal field is predominantly radial, and the two magnetic features that influence the shape of the corona are the closed fields at the base of the corona, and the polarity reversal forming the heliospheric current sheet in the outer corona.

1. Introduction

The highly structured white-light corona unveiled during solar eclipses has had a long history of observation and study. In the absence of measurements of magnetic fields and plasma flow, these images played a major role in our early notions and understanding of the solar magnetic field, as well as the origin and evolution of the solar wind (Hundhausen, 1977; Munro and Jackson, 1977). With dominant features suggestive of diverging polar coronal holes and converging streamers during low solar activity, the solar magnetic field of the inner corona appeared to be highly non-radial.

This paper takes a fresh look at the relationship between magnetic fields and the density structure of white-light images. It has been undertaken for three reasons. First, the density structure of white-light images seems to be organized and shaped by the coronal magnetic field. However, as illustrated in this paper, the structure and its impressions depend on the use of radial gradient filters and image processing. It is, therefore, imperative that we first understand why and how these factors influence images of density structure before inferring magnetic fields from them.

Another way of gaining insight into the topology of the coronal field is to investigate the radial evolution of plasma properties by comparing measurements between the inner and outer corona. When such studies were carried out, the imprint of the base of the corona, comprising signatures of polar coronal holes, the quiet Sun and active regions, was found to appear approximately radially extended in interplanetary space (Woo and Habbal, 1999a,b; Woo, Habbal, and Feldman, 2004). This suggested a solar wind that expanded radially along predominantly open and radial magnetic field lines from all over the Sun, a result that is consistent with the magnetic field direction inferred from polarization measurements (Arnaud and Newkirk, 1987; Eddy, Lee, and Emerson, 1973). The second reason for taking a closer look at white-light images is, therefore, to understand why the impression of non-radial fields in white-light images appears to be at odds with the predominantly radial field inferred from quantitative profiles of white-light measurements.

Recent results based on the synthesis of coronal and *in situ* solar wind measurements have led to progress not only in exploring and defining the distributions of density and flow in the corona, but also in explaining how the solar magnetic field gives rise to them (Woo, Habbal, and Feldman, 2004). The third reason for revisiting white-light images, is, therefore, to capitalize on these gains in knowledge and understanding and elucidate how the density structure captured in white-light images is produced by the solar magnetic field.

2. Solar Eclipse Images

Early hand-drawn pictures of the corona often featured wispy filamentary or raylike structures that extended from the Sun to form large-scale streamers. Although they depend on the visual observer, and the pictures from the same eclipse are often very different, one rendition is presented in Figure 1, which is from Lockyer (1874) and also appears in Foukal (1990). With the advent of photography, solar eclipse images showed a corona that was described by Menzel (1959) as globular in form, with polar rays sometimes visible during solar minimum (Abbott, 1900). In the 1960s, radially graded filters were introduced to compensate for the steep density fall-off, making it possible to image the faint corona farther from the Sun, and reveal an outer corona that was not only filamentary but often spectacular in shape (Newkirk, Dupree, and Schmahl, 1970). When these solar eclipse pictures were further processed to enhance density gradients (Koutchmy, 1977), raylike filamentary structures reminiscent of those in hand-drawn pictures appeared throughout the corona. These features are all evident in the group of solar eclipse images assembled in Figure 2, and taken during solar minimum on June 30, 1973. Why are the impressions of the images of the same corona in Figure 2 so different, and are the density structures all real?

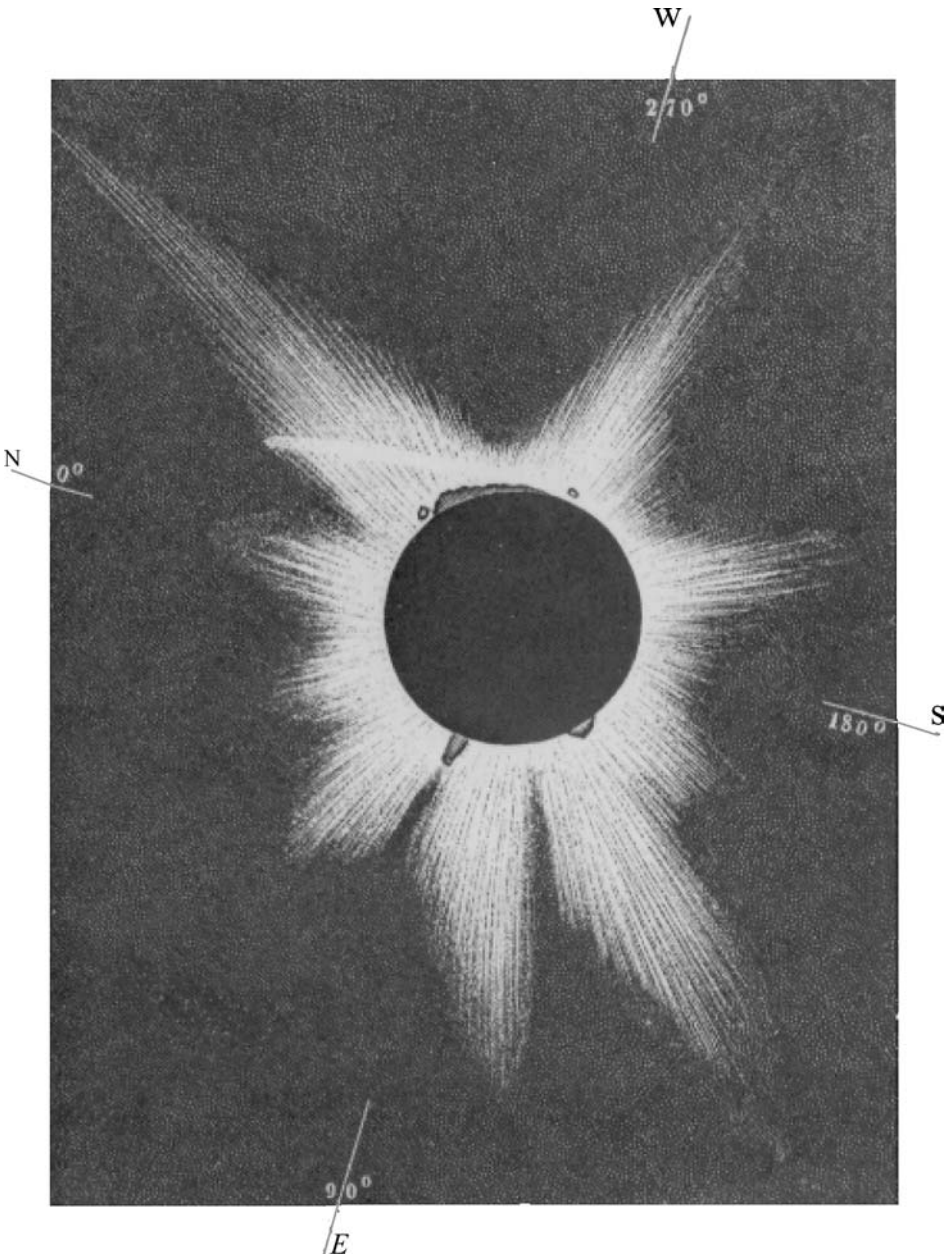

Figure 1. A solar eclipse drawing of the corona of 1868 observed at Mantawalok-Kekee, Malaysia and published by Lockyer (1874). Also reproduced in Foukal (1990).

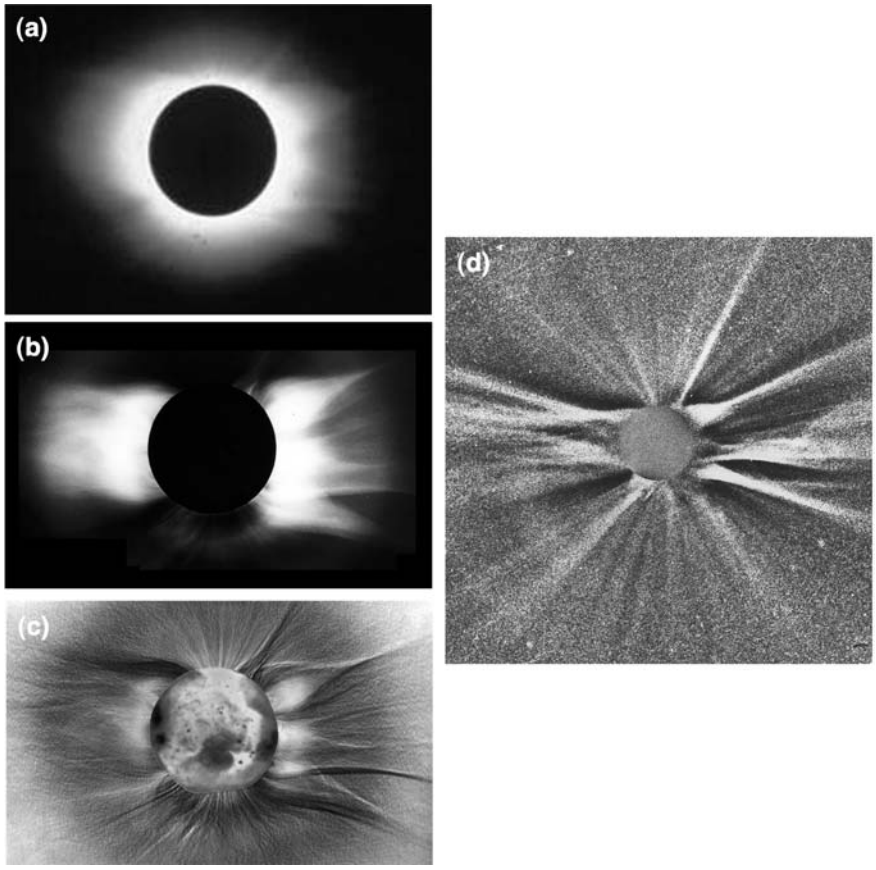

Figure 2. White-light images of the June 30, 1973 solar eclipse. (a) Taken without a radial density gradient filter (courtesy of J. Pasachoff). (b) Taken with the Newkirk camera equipped with a radial density gradient filter by the staff of the High Altitude Observatory. (c) Taken by Koutchmy (1977) and processed to enhance density gradients. (d) Composite of white-light photos taken from an airplane, showing coronal streamers out to 12 $R_{\odot}$ (courtesy of C. F. Keller via J. Pasachoff).

2.1. CORONAL 'SHAPE'

The extent of the corona appears finite in white-light images only because of the rapid fall-off in coronal density with radial distance (see e.g., Waldmeier, 1956), coupled with the inherent limit in sensitivity of the observing instrument. The dark region beyond the globular corona in Figure 2a represents undetected brightness or noise. The variation in coronal extent with latitude, or 'shape' of the corona, therefore, approximates a contour of constant density (isophote) whose level approximates the threshold sensitivity of the instrument. It is clearly not a density feature tracing magnetic field lines. Hereafter in this paper we will use 'shape of corona' and latitudinal variation in coronal extent interchangeably.

The difficulty with imaging the corona is its wide range of light intensity. This stems not only from the steep density gradient in the radial direction, but also from its significant variation with latitude. Both are evident in the measurements of density fall-offs and their differences in polar and equatorial regions during solar minimum (Waldmeier, 1956). To enhance the effective dynamic range of the film by linearizing its response to the disparate intensities of polar and equatorial regions in the outer corona during solar minimum simultaneously, a radially graded filter designed to model the average fall-off of coronal white-light intensity was introduced in the 1960s (see e.g., Newkirk, Dupree, and Schmahl, 1970). As seen in Figure 2b, a radial filter better defines the latitudinal variation of the extent of the corona, and also reveals features suggestive of diverging polar coronal holes (Munro and Jackson, 1977) and tapering streamers (Koutchmy and Lifshits, 1992). However, the fact remains that the shape of the corona outlining these apparent features is still the consequence of the threshold sensitivity of the observing instrument. It is not the result of magnetic fields.

Since the extent of the corona in Figure 2 is shortest in the polar region, the radial filter has the unintended consequence of shifting the apparent extent or boundary of the polar corona at solar minimum closer to the limb of the Sun, and seemingly opening up artificial diverging 'holes' (dark regions) in the polar corona as seen in the comparisons of Figures 2a and 2b. Such apparent diverging holes are present in eclipse pictures taken after the 1960s with the radial filter [see additional images in Figure 3 and in Golub and Pasachoff (1997)], but are absent in those obtained earlier without it [see e.g., the collection of pictures in Menzel (1959)].

The same false impression, that polar coronal holes identified in disk emission measurements extend and diverge in the overlying corona, is evident in white-light images of the ground-based High Altitude Observatory (HAO) Mauna Loa Mk III K–coronameter (Fisher *et al.*, 1981) for which artificial vignetting has been applied to enhance the contrast. An example is shown in Figure 4a. When the levels of brightness and contrast of the Mk III image are increased, the overlying 'missing' corona becomes visible, as seen in Figure 4b, in agreement with the presence of corona detected at those heights in the latitudinal profiles of density (see e.g., Woo and Habbal, 1999b). These results illustrate that the white-light corona observed by a sensitivity-limited instrument above polar coronal holes identified in disk emission measurements, is not characterized by a hole in the corona that diverges with radial distance. Rather, it is characterized by the shortest extent of the corona.

2.2. Fields and flow relative to coronal shape

The availability of solar wind speeds inferred from Doppler dimming measurements by the SOHO Ultraviolet Coronagraph Spectrometer (UVCS) (Kohl *et al.*, 1995)

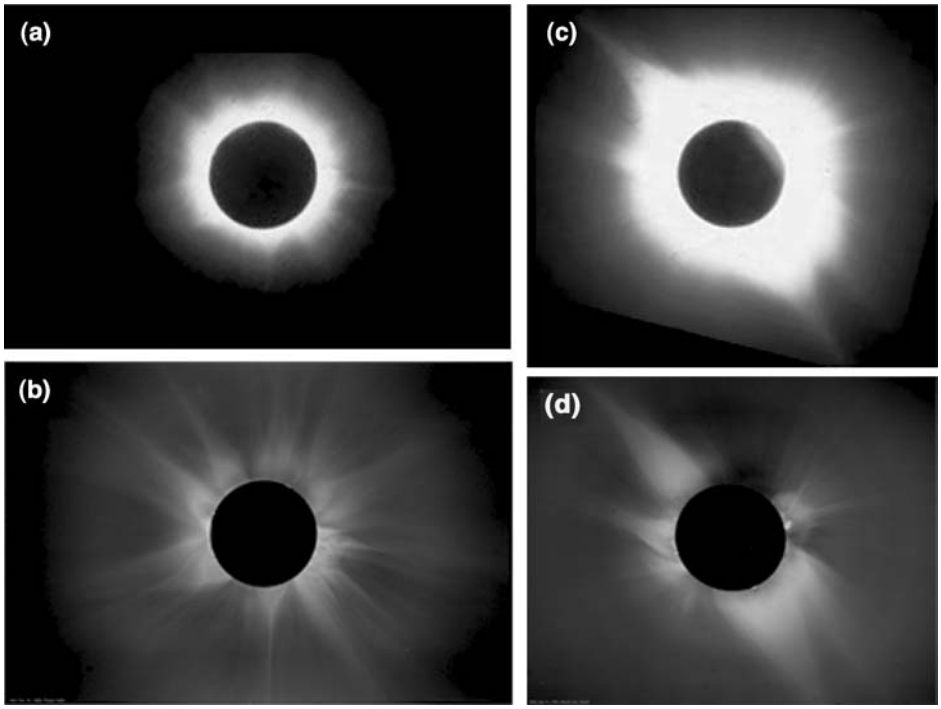

Figure 3. White-light image of the February 16, 1980 solar eclipse: (a) taken without radial density gradient filter (courtesy of J. Pasachoff), and (b) taken with the Newkirk camera by the staff of HAO. White-light image of the 11, July 11, 1991 solar eclipse: (c) taken without radial density gradient filter (courtesy of J. Pasachoff), and (d) with the Newkirk camera by the staff of HAO.

makes it possible to relate density structure to plasma flow. Shown in Figure 5 is the constant velocity contour of January 17, 1997 corresponding to approximately 94 km s^{-1} obtained by Habbal *et al.* (1997), and superposed on combined white-light images from the HAO Mauna Loa Mk III K–coronameter (Figure 4b) and the SOHO Large Angle Spectrometric Coronagraph (LASCO) C2 (Brueckner *et al.*, 1995). Since the wind is still accelerating at 94 km s^{-1}, the contour of constant velocity indicates how solar wind acceleration varies with latitude. The approximate boundary of detection of the Mk III image continues as that of the brightest corona in the C2 image, and is an approximate contour of constant density. The striking similarity in shapes of the density and velocity contours reinforces the anticorrelation between density and velocity in the solar corona (Woo and Habbal, 2000), and implies that the coronal shape conveys information on wind acceleration as well. It also demonstrates that, since the shape of the corona approximates the contour of constant velocity, the diverging streamer boundary cannot represent the plasma flow line of an accelerating wind.

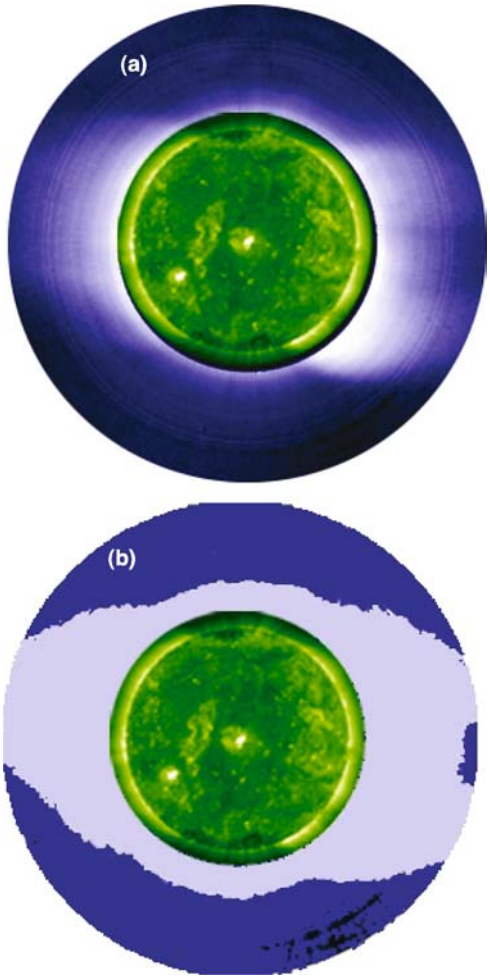

Figure 4. (a) White-light image of January 17, 1997 taken by the HAO Mauna Loa Mk III K–coronameter (Fisher *et al.*, 1981) and displayed with artificial vignetting applied to reduce the dynamic brightness range. (b) Same as (a) except brightness and contrast increased to reveal the radial extent of the detected corona.

Simultaneous polarization and white-light measurements also make it possible to relate density structure of white-light images to magnetic field direction. These comparisons have shown that the predominantly radial magnetic field does not trace the non-radial boundaries of coronal streamers (Habbal, Woo, and Arnaud, 2001). Polarization (of field direction) and Doppler dimming (of plasma flow) measurements, therefore, support the notion that the shape of the corona is not a consequence of non-radial fields or non-radial flow. In the next section, we will discuss how the coronal shape is produced by the solar magnetic field.

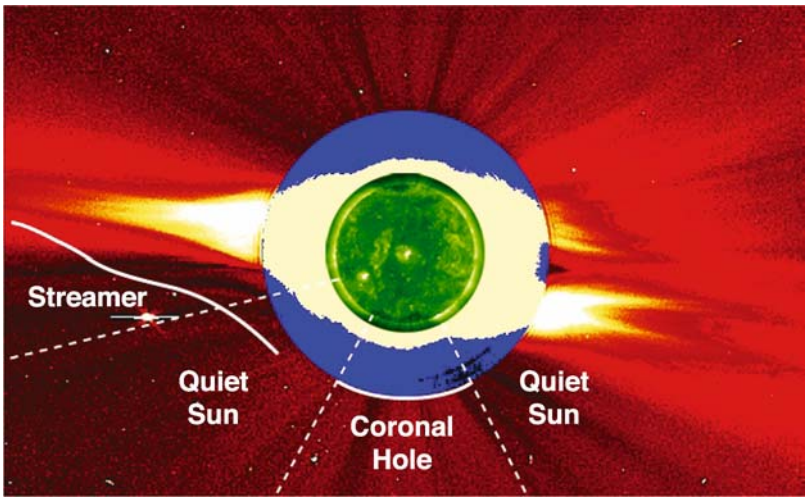

Figure 5. Mk III image of Figure 4b combined with LASCO C2 image of January 17, 1997. The white line is the constant velocity contour of 94 km s^{-1} inferred from Doppler dimming measurements by Habbal *et al.* (1997). The dashed lines delineate the coronal hole, quiet Sun and streamer regions. The latitudinal density profile at the base of the corona is replicated in the outer corona in the coronal hole and quiet Sun.

3. How the Magnetic Field Produces the Shape of the Corona

Instead of highly non-radial structures, the inner corona comprises ubiquitous filamentary structures that trace the predominantly radial and open magnetic field lines observed in polarization measurements, as portrayed in Figure 1, and the solar wind expands radially from the Sun. This picture has been constructed through the synthesis of coronal and solar wind measurements including quantitative profiles of white-light measurements (Woo and Habbal, 2003). Furthermore, composition measurements have shown how the presence of closed fields and their ability to trap plasma at the base of the corona for prolonged periods control the plasma properties of the radially expanding wind (Woo, Habbal, and Feldman, 2004). As a measure of confinement time, first ionization potential (FIP) bias represents an observed property of the interaction between the magnetic field and its surrounding plasma that is directly related to plasma flow and density fall-off observed in the overlying corona. Density fall-off is the key coronal characteristic used in constructing this picture. Since the shape or radial extent of the corona depends on the combination of density at the base of the corona and its fall-off, the coronal shape can be related to, and also explained by, this picture.

3.1. Coronal shape and radially expanding wind

The nearly photospheric composition (FIP bias $\sim$1) of the radially expanding and accelerating solar wind, which emerges from the polar coronal hole and

high-latitude quiet Sun regions delineated in Figure 5, indicates the absence of prolonged plasma trapping by closed fields at the base of the corona (Woo, Habbal, and Feldman, 2004). Without trapping, flow is least impeded, and density fall-off is steepest (Waldmeier, 1956). The former explains why the radial distance of the 94 km s^{-1} velocity contour in Figure 5 is shortest over the polar coronal hole, and the latter why the radial extent of the white-light corona in Figure 5 is shortest over the polar coronal hole.

The corona extends slightly farther, and the velocity contour reveals that the wind acceleration is slightly slower, in the quiet Sun than in the polar coronal hole. This is explained by the fact that the radial density gradient is uniform in the absence of plasma trapping (Woo, Habbal and Feldman, 2004), so that the extent of the corona over the quiet Sun reflects the higher density at its base due to the enhanced presence of closed fields. These closed fields also give rise to the slightly slower wind acceleration.

The longer radial extensions of the corona in the 'streamer region' reflect the significantly shallower radial density gradients resulting from the trapping of plasma by closed fields at the base of the corona. Prolonged plasma trapping is characterized by FIP bias >1 (Sheeley *et al.*, 1995). The strong latitudinal variations in coronal extent are indicative of the non-uniformity of the density gradients, and explain why the density profile at the base of the streamer region is not replicated in the outer corona (Woo and Habbal, 1999b). The non-uniform coronal extensions result from variations in plasma confinement time or variations in FIP bias: the longer the confinement time, the higher the FIP bias, the longer the coronal extension, and the slower the wind acceleration.

To explain the quantitative radial density profiles obtained from white-light measurements in terms of this picture, we consider the conservation of particles in a flow tube of cross-section $A(r)$, i.e.

$$N(r)V(r)A(r) = \text{constant} \tag{1}$$

where N is density and V is flow speed, and both vary with radial distance r. In a radially expanding solar wind for which A varies as r^2, density will vary as $1/r^2$ when acceleration is essentially complete in the outer corona, i.e. when $V(r)$ becomes almost constant. By contrast, in the immediate vicinity of the Sun where the wind is still accelerating, i.e. $V(r)$ increases with r as r^n, and $N(r)$ falls off more rapidly as $1/r^{2+n}$. Because acceleration is fastest in polar coronal holes, density profiles are steeper (and steepest and closest to the Sun) in polar coronal hole than equatorial regions (Waldmeier, 1956; Billings, 1966; Fisher and Guhathakurta, 1994). With the completion of wind acceleration closest to the Sun in polar coronal holes (Grall *et al.*, 1996), density fall-off also reaches $1/r^2$ closest to the Sun in polar coronal holes (Guhathakurta and Fisher, 1998).

3.2. HELIOSPHERIC CURRENT SHEET

Despite the impression of white-light images, especially those enhancing density gradients such as Figure 2b, the streamer is not a monolithic large-scale feature that tapers to the narrowest and farthest-reaching feature often identified as a stalk (Koutchmy and Lifshits, 1992). Instead, the stalk is a distinct and separate density feature that encompasses the magnetic field polarity reversal, as confirmed by Faraday rotation measurements of the corona (Woo, 1997). It represents the heliospheric current sheet (HCS) when viewed edge on. The HCS dominates the outer corona of white-light measurements, as evident in Figures 2–5, and demonstrated by Wang *et al.* (1997). It also dominates Doppler scintillation measurements, because it comprises fine-scale filamentary structures with the strongest transverse density gradients (Woo *et al.*, 1995).

The reason the HCS dominates density measurements of the outer corona is that the presence of the polarity reversal slows down the fall-off in density so that the radial density gradient is shallower than the $1/r^2$ of the rest of the outer corona. So overwhelming is its brightness that the HCS masks the radial extension of polar coronal holes in images obtained by SOHO LASCO. Only when the gain is increased so that the brightness of the low-latitude streamers is saturated does the radial extension of polar coronal holes become visible in the image [see Figure 1 of Woo *et al.* (1999)].

As implied by the farthest distance of the velocity contour in Figure 5, acceleration is slowest in the streamer stalk. This is also evident when the acceleration profile of slow wind along streamer stalks inferred from time-lapse sequences of white-light measurements (Sheeley *et al.*, 1997) is compared with that of the fast wind (Grall *et al.*, 1996).

The close relationship between coronal streamer structure and in situ measurements of the HCS has long been recognized (Gosling *et al.*, 1981; Bavassano, Woo, and Bruno, 1997; Wang *et al.*, 2000). It is clear from Figure 5 that the HCS organizes and gives rise to distinct and narrow signatures in density and flow. That the HCS at 1 AU is still characterized by a narrow signature in density (because of its shallowest density gradient) but not in velocity (Gosling *et al.*, 1981, Winterhalter *et al.*, 1994), suggests that within the HCS, the slow wind must continue to accelerate farther from the Sun than the slow wind outside the HCS. That the more slowly accelerated slow wind within the HCS catches up to the faster accelerated slow wind outside the HCS, is the likely reason why *Ulysses* found a broad minimum of solar wind speed in the streamer belt, and why the minimum speed locus did not coincide with the HCS (Crooker *et al.*, 1997; Neugebauer *et al.*, 1998).

4. Small-Scale Structures

Highly sensitive and high-resolution radio occultation measurements have shown that the solar corona is permeated by small-scale raylike or filamentary structures.

These span a wide range of scale sizes with the smallest being about a kilometer, and are characterized by small differences in brightness (low contrast) bound by steep transverse gradients (Woo, 1996a,b). For this reason, they are revealed when white-light images such as Figure 2b are processed to enhance density gradients, as evident in Figure 2c (Koutchmy, 1977). With improvements in spatial resolution, signal-to-noise ratio, and processing techniques, more recent images show finer details, as evident in Figure 6. The processed images also have the unintended consequence of highlighting the artificial boundaries of diverging polar coronal holes and tapering coronal streamers, thus accentuating the false impression that holes and streamers are monolithic features of the inner corona. That the corona is permeated by ubiquitous and predominantly radial filamentary structures, is also evident by the fact that they always appear at the extensions of coronal images, where threshold sensitivity makes the low-contrast structures more visible. Low-contrast polar plumes are more visible in the tenuous polar regions of the corona for the same reason.

At first sight, polar plumes (DeForest *et al.*, 1997), which may be tracing a large-scale dipolar-like magnetic field, seem to be at odds with a radially expanding polar wind. One explanation is that they could be representing the tops of large arcades of closed loops at high latitude, and another might be that they are simply lower-latitude 'streamers' seen in projection in the polar regions (Li, Jewitt, and LaBonte, 2000). Their precise nature, however, is not crucial for determining the overall extension of the corona, because polar plumes represent only a few of the low-contrast structures in the corona. Unseen in white-light images, because they are either too small or have too low a contrast to be detected, are the ubiquitous ultra-fine scale filamentary structures detected by highly sensitive radio occultation measurements (Woo, 1996a,b). The more robust evidence for the radial extension of the polar corona comes from the replication of the inner corona density profile in the outer corona, which includes all structures, a result that is not significantly affected by the presence of a few plumes representing $\pm 10\%$ variations of the profile (Fisher and Guhathakurta, 1995; Woo, 1996c; Woo and Habbal, 1999a). A large-scale dipolar-like field may very well be present at the same time, but observations of the consequences of the solar magnetic field indicate that the radial component, and not the non-radial component, dominates the evolution of solar wind properties.

Spectroscopic measurements are selective because they sense filamentary structures at specific wavelengths. In regions of mixed (interspersed) open and closed fields, they favor the hotter and denser closed structures whose emission is strongest. On the contrary, white-light measurements observe all structures, regardless of their temperature or whether they are open or closed. It is for this reason that processed images such as Figure 6 reveal both closed and open structures, and give a truer impression of an open corona interspersed with low lying closed structures. In the case of LASCO on SOHO, because C1 observes emission and C2 and C3 observe white-light, combining such images tends to reinforce the false impression of diverging polar coronal holes (Schwenn *et al.*, 1997).

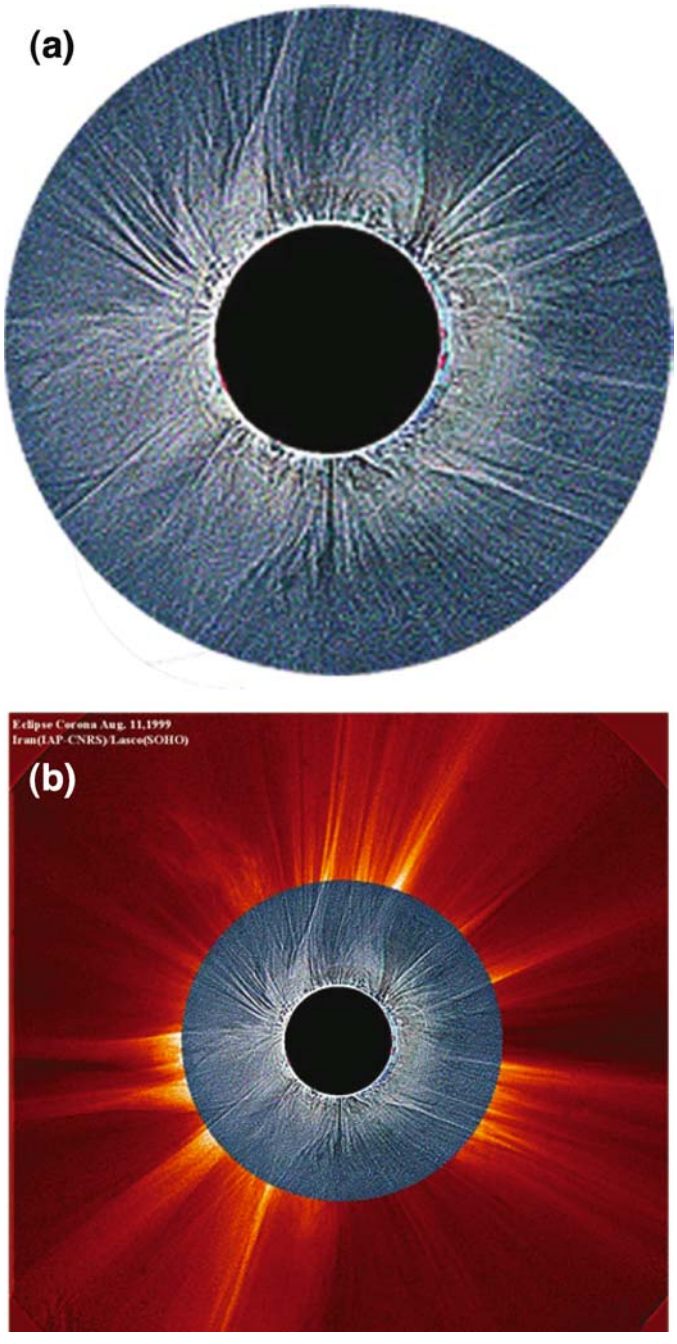

Figure 6. White-light images of the August 11, 1999 solar eclipse. (a) Taken by and courtesy of S. Koutchmy, processed to enhance density gradients. (b) Image of (a) combined with image from SOHO LASCO C2 also processed to enhance density gradients, courtesy of S. Koutchmy.

5. Discussion and Conclusions

We have discussed how the use of a radial graded density filter defines the shape of the corona in solar eclipse pictures more precisely, revealing features suggestive of diverging polar coronal holes and converging coronal streamers. However, the fact remains that the boundaries of these features still represent the latitudinal variation in the extent of the corona detected by an observing instrument with limited sensitivity, and that they are not shaped by non-radial magnetic fields. This is reinforced by the fact that polarization measurements of magnetic field direction, and Doppler dimming measurements of solar wind speed, show that the boundaries of the apparent diverging polar coronal holes and converging streamers are neither magnetic field lines nor plasma flow lines.

Instead, when integrated with earlier measurements and results showing that the coronal field is predominantly radial, it is found that the two magnetic features that influence the shape of the corona are the closed fields at the base of the corona, and the magnetic field polarity reversal that forms the heliospheric current sheet. The presence of closed fields and their ability to confine plasma for prolonged periods produces the coupled variations in radial extent and wind acceleration.

The heliospheric current sheet hinders density fall-off and acceleration of the solar wind, giving rise to the shallowest density fall-off and slowest acceleration. This explains why the heliospheric current sheet dominates the outer corona of white-light images as linear structures, or streamer stalks when the current sheet is viewed edge-on. Continuing acceleration along the current sheet allows it to catch up with the faster slow wind surrounding it, resulting in the relatively wide band of slow wind observed in the streamer belt at 1 AU.

Small-scale filaments are revealed when images are processed to enhance density gradients, because they are low-contrast structures bound by steep gradients. They are also seen in the extensions of the corona, and in tenuous polar coronal hole regions, where the closeness of their brightness to the sensitivity threshold of the instrument makes them more visible. In the images processed to enhance gradients, the false impression of diverging polar coronal holes and converging streamers is accentuated, but the predominance of open and nearly radial structures is consistent with the radially expanding wind.

The advantage of using radial density gradient filters or processing images to enhance density gradients is that the results present a corona whose structure is closer to that seen by the naked eye. Compared with film and print images, the eye has an enormous dynamic range, and an outstanding ability to distinguish small differences in brightness. However, as Menzel (1959) pointed out long ago: "While the eye in some ways gives a truer impression of the overall corona, it is in other ways a poor judge of coronal brightness because it tends to exaggerate small differences. If even in the most jagged-appearing corona, we determine an exact contour of equal intensity (a so-called isophote) the line is surprisingly round and symmetrical. The most brilliant streamer shows only as a slight bump in the

otherwise smooth contour. Thus the corona is actually surprisingly close to globular in form."

Imaging and quantitative profiles complement each other, and both are necessary for understanding coronal structure. The complex corona is a mixture of open and closed, radial and non-radial structures, and individual structures in images such as polar plumes represent only a few of the ubiquitous small-scale structures, most of which are not detected in white-light images. However, the picture of a highly filamentary corona that expands radially from the Sun, explains the effects of radial gradient filters and image processing on the density structure of white-light images, reconciles the apparent conflict between evidence for seemingly highly non-radial magnetic fields in images and that of a predominantly radial field from quantitative profiles of white-light measurements, and improves our understanding of how the density structure of white-light images is produced by, and related to, coronal magnetic fields and plasma flow.

Acknowledgments

This research was carried out at the Jet Propulsion Laboratory, California Institute of Technology, under a contract with the National Aeronautics and Space Administration. I am grateful to S. Koutchmy and J. Pasachoff for kindly making available their solar eclipse pictures. I would like to acknowledge the JPL sabbatical program that made this work possible, and to express my appreciation to the hosts: S. Habbal of University of Wales, Aberystwyth, M. Kojima of STELab, Nagoya University, L. Iess of Università di Roma "La Sapienza," and E. Rhodes, Jr. of University of Southern California. Finally, it is a pleasure to thank J.W. Armstrong and S.R. Habbal for stimulating and useful discussions.

References

Abbott, C. G.: 1900, *Astrophys. J.* **12**, 69.
Arnaud, J. and Newkirk, G., Jr.: 1987, *Astron. Astrophys.* **178**, 263.
Bavassano, B., Woo, R., and Bruno, R.: 1997, *Geophys. Res. Lett.* **24**, 1655.
Billings, D. E.: 1966, *Solar Corona*, Academic Press, New York.
Brueckner, G. E., *et al.*: 1995, *Solar Phys.* **162**, 357.
Crooker, N. U., *et al.*: 1997, *J. Geophys. Res.* **102**, 4673.
DeForest, C. E., *et al.*: 1997, *Solar Phys.* **175**, 393.
Eddy, J. A., Lee, R. H., and Emerson, J. P.: 1973, *Solar Phys.* **30**, 351.
Fisher, R., Lee, R. H., MacQueen, R. M., and Poland, A. I.: 1981, *Appl. Opt.* **20**, 1094.
Fisher, R. and Guhathakurta, M.: 1994, *Space Sci. Rev.* **70**, 267.
Foukal, P.: 1990, *Solar Astrophysics*, Wiley, New York, 12.
Golub, L. and Pasachoff, J. M.: 1997, *The Solar Corona*, Cambridge University Press, Cambridge.
Gosling, J. T., *et al.*: 1981, *J. Geophys. Res.* **86**, 5438.

Grall, R. R., *et al.*: 1996, *Nature* **379**, 429.
Guhathakurta, M. and Fisher, R.: 1998, *Astrophys. J.* **499**, L215.
Habbal, S. R., *et al.*: 1997, *Astrophys. J.* **489**, L103.
Habbal, S. R., Woo, R., and Arnaud, J.: 2001, *Astrophys. J.* **558**, 852.
Hundhausen, A.: 1977, in J. B. Zirker (ed.), *Coronal Holes and High Speed Streams*, Colorado Associated University Press, Boulder, CO, p. 225.
Kohl, J. L., *et al.*: 1995, *Solar Phys.* **162**, 313.
Koutchmy, S.: 1977, *Solar Phys.* **51**, 399.
Koutchmy, S. and Lifshits, M.: 1992, *Space Sci. Rev.* **61**, 393.
Li, J., Jewitt, D., and LaBonte, B.: 2000, *Astrophys. J.* **539**, L67.
Lockyer, J. N.: 1874, *Contributions to Solar Physics,* Macmillan, London.
Menzel, D. H.: 1959, *Our Sun*, Harvard University Press, Cambridge.
Munro, R. and Jackson, B.: 1977, *Astrophys. J.* **213**, 874.
Neugebauer, M., *et al.*: 1998, *J. Geophys. Res.* **103**, 14587.
Newkirk, G., Jr., Dupree, R. G., and Schmahl, E. J.: 1970, *Solar Phys.* **15**, 15.
Schwenn, R., *et al.*: 1997, *Solar Phys.* **175**, 667.
Sheeley, N. R., Jr., *et al.*: 1997, *Astrophys. J.* **484**, 472.
Waldmeier, M.: 1956, *Z. Astrophys.* **40**, 120.
Wang, Y.-M., *et al.*: 1997, *Astrophys. J.* **485**, 875.
Wang, Y.-M., Sheeley, N. R., Jr., Socker, D. G., Howard, R. A., and Rich, N. B.: 2000, *J. Geophys. Res.* **105**, 25133.
Winterhalter, D., Smith, E. J., Burton, M. E., and Murphy, N.: 1994, *J. Geophys. Res.* **99**, 6667.
Woo, R.: 1996a, in D. Winterhalter, J. T. Gosling, S. R. Habbal, W. S. Kurth, and M. Neugebauer (eds.), *Solar Wind Eight*, AIP, New York, p. 38.
Woo, R.: 1996b, *Nature* **379**, 321.
Woo, R.: 1996c, *Astrophys. J.* **464**, L95.
Woo, R.: 1997, *Geophys. Res. Lett.* **24**, 97.
Woo, R. and Habbal, S. R.: 1999a, *Astrophys. J.* **510**, L69.
Woo, R. and Habbal, S. R.: 1999b, *Geophys. Res. Lett.* **26**, 1793.
Woo, R. and Habbal, S. R.: 2000, *J. Geophys. Res.* **105**, 12667.
Woo, R. and Habbal, S. R.: 2003, in M. Velli, R. Bruno, and F. Malara (eds.), *Solar Wind Ten*, AIP, New York, p. 55.
Woo, R., Habbal, S. R., and Feldman, U.: 2004, *Astrophys. J.* **612**, 1171.
Woo, R., Armstrong, J. W., Bird, M. K., and Pätzold, M.: 1995, *Astrophys. J.* **449**, L91.
Woo, R., Habbal, S. R., Howard, R. A., and Korendyke, C. M.: 1999, *Astrophys. J.* **513**, 961.